

Electroosmotic flow steers neutral products and enables concentrated ethanol electroproduction from CO₂

Rui Kai Miao, Yi Xu, Adnan Ozden, Anthony Robb, Colin P. O'Brien, Christine M. Gabardo, Geonhui Lee, Jonathan P. Edwards, Jianan Erick Huang, Mengyang Fan, Xue Wang, Shijie Liu, Yu Yan, Edward H. Sargent, and David Sinton

Version Post-print/Accepted Manuscript

Citation Miao, R.K., Xu, Y., Ozden, A., Robb, A., O'Brien, C.P., Gabardo, C.M., Lee, G., Edwards, J.P., Huang, J.E., Fan, M., Wang, X., Liu, S.,
(published version) Yan, Y., Sargent, E.H., Sinton, D. (2021). Electroosmotic flow steers neutral products and enables concentrated ethanol electroproduction from CO₂. *Joule* 5, 2742–2753.
<https://doi.org/10.1016/j.joule.2021.08.013>

Copyright/License



This work is licensed under the Creative Commons Attribution-NonCommercial-NoDerivatives 4.0 International License. To view a copy of this license, visit [Creative Commons BY NC ND 4.0 License](https://creativecommons.org/licenses/by-nc-nd/4.0/).

How to cite TSpace items

Always cite the published version, so the author(s) will receive recognition through services that track citation counts, e.g. Scopus. If you need to cite the page number of the **author manuscript from TSpace** because you cannot access the published version, then cite the TSpace version **in addition to** the published version using the permanent URI (handle) found on the record page.

This article was made openly accessible by U of T Faculty.

Please [tell us](#) how this access benefits you. Your story matters.

Electroosmotic flow steers neutral products and enables concentrated ethanol electroproduction from CO₂

Rui Kai Miao,^{1,3} Yi Xu,^{1,3} Adnan Ozden,¹ Anthony Robb,¹ Colin P. O'Brien,¹ Christine M. Gabardo,¹ Geonhui Lee,² Jonathan P. Edwards,¹ Jianan Erick Huang,² Mengyang Fan,¹ Xue Wang,² Shijie Liu,¹ Yu Yan,² Edward H. Sargent,² and David Sinton^{1,4,*}

¹Department of Mechanical and Industrial Engineering, University of Toronto, 5 King's College Road, Toronto, Ontario, M5S 3G8, Canada.

²Department of Electrical and Computer Engineering, University of Toronto, 10 King's College Road, Toronto, Ontario, M5S 3G4, Canada.

³These authors contributed equally to this work.

⁴Lead contact*Correspondence: sinton@mie.utoronto.ca

SUMMARY

Electrochemical reduction of carbon dioxide (CO₂RR) converts intermittent renewable energy into high energy density fuels, such as ethanol. Membrane electrode assembly (MEA) electrolyzers are particularly well-suited to CO₂-to-ethanol conversion in view of their low ohmic resistance and high stability. However, over 75% of the ethanol produced at the cathode migrates through the membrane where it is diluted by the anolyte and may be oxidized. The ethanol concentration that results is two orders of magnitude below the 10 wt% standard set by the incumbent industrial process, fermentation. Here, we reverse the direction of ion and electroosmotic transport by means of a porous proton exchange layer, and thereby block both the convective and diffusive routes of ethanol loss. With this strategy, we eliminate ethanol crossover to the anode (< 1%), and achieve an ethanol concentration of 13.1 wt% directly from the cathode outlet.

CO₂ electroreduction; carbon utilization; catalysis; electrolyzer; ethanol; concentration; downstream separation; liquid crossover; polymer electrolyte; membrane electrode assembly;

INTRODUCTION

A transition from fossil fuels to renewables will require large-scale storage of intermittent renewable energy.^{1,2} Electrochemical CO₂ reduction reaction (CO₂RR) provides a promising route to convert renewable electricity into valuable and storable multi-carbon products.^{3,4} Compared to gaseous-phase products, liquid oxygenates such as ethanol have a high volumetric energy density that enables easy storage and transport.⁵ Ethanol is an important commodity fuel (26.8 MJ/kg),⁶ and is currently produced through processes that are energy-intensive and carbon-positive.⁷ With recent advances in CO₂RR catalysts, the electroproduction of ethanol approaches industrially-relevant production rates and selectivities.⁸⁻¹⁰

Membrane electrode assembly (MEA) electrolyzers are reaction platforms that, when equipped with highly active and selective catalysts, enable CO₂-to-ethanol conversion at high current densities and selectivities.⁸ In these systems, the anode and cathode are separated by an anion exchange membrane (AEM), reducing ohmic resistance and increasing overall energy efficiency.^{11,12} In the absence of an electrolyte on the cathode side, MEAs present an opportunity for the direct production of concentrated liquid products at the cathode.¹³ In contrast, conventional liquid flow-cell electrolyzers dilute cathode products in bulk electrolyte, requiring extensive downstream separation.^{14,15}

In practice, ethanol-producing MEA systems have suffered liquid product crossover. Concentrated liquid products formed at the cathode migrate through the membrane – via electroosmotic drag and diffusion¹⁶⁻¹⁸ – to the anode side where they are either oxidized or

diluted in the bulk anolyte. At industrially relevant reaction rates ($>100 \text{ mA/cm}^2$), up to 75% of the ethanol produced at the cathode passes through the AEM limiting the recoverable ethanol yield (Figure 1A). The ethanol concentrations in the anolyte are generally in the range of 0.05 wt%. Recovering ethanol from such low concentration streams is not practical, incurring a downstream separation energy penalty that exceeds the product value.^{14,19} Industrial bioethanol processes provide ethanol at $\sim 10 \text{ wt}\%$,²⁰ setting a benchmark concentration for electrocatalytic production that is 200-fold that of current electrolyzer anolytes. Increasing product stream concentrations and reducing energetic losses are critical for the feasibility of CO_2 -to-ethanol conversion.

Several approaches have been developed to increase concentrations of liquid CO_2 RR products. Tuning the electrolyzer temperature¹³ and the polarity of the membrane (cationic and anionic)^{21–23} has resulted in higher output concentrations, as have dedicated liquid product collection substrates.^{24–26} These approaches have resulted in record concentrations of 4 wt% for ethanol, 7 wt% for acetate, and 100 wt% for formate. The 4 wt% ethanol stream constituted only 60% of the ethanol produced, with the remainder lost to the anode.¹³ The remarkable concentration of formate was possible due to the charged nature of the product.²⁴ Electroneutral products such as ethanol cannot be directly steered by the applied field, and transport efficiently through membranes via diffusion and electroosmotic drag.

Here we present an electrolyzer system that simultaneously blocks ethanol crossover and enables its direct collection from the cathode at concentrations exceeding that the incumbent—industrial fermentation-based ethanol production. We reverse the direction of electroosmotic transport at the anode via a porous proton exchange layer and thereby block both the convective and diffusive ethanol crossover mechanisms. We demonstrate an ethanol crossover loss below 1%, and by further tuning the flow rate in the porous layer and the temperature of the cell, achieve direct production of a 13.1 wt% ethanol stream.

RESULTS AND DISCUSSION

Crossover in the MEA

To establish a baseline and assess the energy penalty associated with the crossover of produced ethanol, we first performed experiments in the conventional MEA electrolyzer, having only an AEM (Figure 1A). We employed a Cu sputtered polytetrafluoroethylene (PTFE) gas diffusion electrode due to its stable selectivity toward ethanol.¹³ The degree of crossover was measured for a wide range of current densities from 100 mA/cm^2 to 300 mA/cm^2 with 0.1 M KHCO_3 anolyte. We measured the selectivity toward ethanol by collecting the products simultaneously from the cathodic and anodic streams (Figure 1B). Continuous monitoring of CO_2 RR products at the cathodic and anodic streams enabled us to quantify the extent of ethanol crossover. The total ethanol Faradaic efficiency (FE) increased with increasing current density, reaching a maximum FE of 23% at 250 mA/cm^2 (Figure S5C). Increasing the current density resulted in increased hydrogen production and lowered the FE toward ethanol (Figure 5S). The degree of ethanol crossover (fraction of ethanol that was detected in the anolyte) remained relatively constant and exceeded 75% for all current densities screened (Figure 1B). This analysis of all streams confirms that the majority of produced ethanol migrated through the AEM to the anode and was diluted in the large volume of anolyte—a finding in keeping with previous works.¹³ The concentration of ethanol inside the anolyte (200 mL) was determined to be less than 0.05 wt% after a 5-h of continuous electrolysis at 200 mA/cm^2 (Figure S3). Ethanol produced at this concentration is not practical to recover, and is a waste stream.¹⁴ Extending the electrosynthesis duration or decreasing the total volume of anolyte would increase the concentration of ethanol in the anolyte. However, such a strategy would suffer the secondary loss mechanism, oxidation of ethanol back to CO_2 . Iridium-based catalysts show catalytic activity for ethanol oxidation at even moderately higher concentrations (0.5 wt%).^{27,28}

We performed further control experiments in which ethanol at different concentrations (0.1 wt%, 0.5 wt%, and 1 wt%) was added directly to the anolyte while the cathode was operated under HER conditions (200 mA/cm^2) to avoid the generation of additional ethanol (Figure 1C and Figure S4). We confirmed oxidation of ethanol in the anolyte at all concentrations operated and the rate of oxidation increased with the concentration of the ethanol in the anolyte. At a concentration of 0.5 wt% in the anolyte, the rate of ethanol oxidation loss exceeded the CO_2 RR production rate of ethanol achieved in earlier tests (20%

FE at 200 mA/cm²). Ethanol in the anolyte was either partially oxidized to acetate and acetaldehyde or completely to CO₂ (Figure S4), consistent with previous reports.^{29,30} These tests indicate that ethanol concentration in the anolyte will be limited to less than 0.5 wt%, a concentration well below the practical threshold of 10 wt%. The majority of ethanol produced in conventional MEA systems is lost to a combination of dilution and oxidation.

The electrolyzer with the porous proton exchange layer

The crossover of electroneutral ethanol results from a combination of convection and diffusion. Convective loss of ethanol results from the electroosmotic drag of the negatively charged ions (hydroxide, carbonate, and bicarbonate) in response to the electric field, through the anion-selective membrane. Diffusive loss of ethanol results from the concentration gradient and high permeability of the membrane. These loss mechanisms are particularly strong in the case of ethanol due to its electroneutral, polar and highly solvating nature. We reasoned that reversing the direction of the electroosmotic flow would remove the convective transport mechanism and also block diffusion via oncoming flow. Reversing the ion flow at the anode would require a proton flux from the anolyte, and a mediating proton exchange layer (Figure 2A and Figure S2). We integrated a porous proton-conducting layer^{26,31} placed directly between an AEM and a cation exchange membrane (CEM) to allow direct ion conduction from the anode to cathode, in the direction opposite to ethanol crossover. The AEM provided a local alkaline environment at the cathode catalyst surface to minimize the hydrogen evolution reaction (HER) and facilitate C-C coupling to multi-carbon products.³²⁻³⁴ The microscale proton conductors (averaging 50 μm in diameter, Figure S1) were tightly packed between the AEM and CEM to facilitate surface-based proton conduction from CEM to AEM. The porous layer also facilitated collection of ethanol that migrated across the AEM. Ethanol within the layer could be removed by flushing with an inert gas flow or deionized (DI) water. The CEM ensured the proton flux and prevented direct mixing of the liquid products with the anolyte. DI water or sulphuric acid (0.01M H₂SO₄) was used as anolyte without introduction of salt to eliminate salt-precipitation stability issues³⁵ and avoid any potential contamination of the produced ethanol stream³⁶.

Performance of the electrolyzer with the porous proton exchange layer

To enable a direct comparison with the conventional AEM-based system, we employed the same ethanol-producing cathode catalyst in the electrolyzer with the porous proton exchange layer. We first characterized the current response by varying the full-cell voltage from -3.6 to -5V at room temperature (Figure 2B). Although the additional thickness of the porous layer introduced additional ohmic losses between the electrodes, the overall current density exceeded 200 mA/cm² at a full-cell voltage of -4.7V (Figure 2B).

The generated gas products were monitored over the same voltage range (Figure 2C). The selectivity toward carbon monoxide (CO) decreased continuously with increasing cell voltage and current density, and the CO FE was lower than 10% at a voltage of -4.8V. The reduction in the CO FE coincided with an increase in the FE toward ethylene (C₂H₄), reaching a maximum FE of 50% at -4.8V. The competing HER was suppressed to under 12% for all current densities up to 200 mA/cm².

The selectivity for liquid products increased with increasing voltage, with ethanol as the predominant liquid product (Figure 2D). The selectivity of ethanol followed a similar trend as C₂H₄, reaching a maximum FE of 21% at -4.9V, corresponding to a partial ethanol current density of 46 mA/cm². The production of other liquid products (formate, acetate, and n-propanol) remained relatively constant over the range of applied voltage. Compared to the performance of the AEM-based MEA (Figure S5), selectivity toward all gas and liquid products showed similar trends, indicating that the porous proton exchange layer did not alter the cathodic reaction environment significantly.

Next, we assessed the ethanol crossover performance of the electrolyzer by measuring the ethanol content at the outlets of the cathode, the porous layer, and the anode (Figure 2E). Ethanol passing through the AEM was captured by the porous layer, and crossover to the anode was blocked, with < 1% of produced ethanol detected in the anolyte over the full range of current densities from 100 to 300 mA/cm². The porous layer also suppressed the crossover of other CO₂RR liquid products (formate, acetate, n-propanol) to the anolyte

(Figure S6). This result highlights the effectiveness of this approach in preventing liquid product crossover to the anode, as well as the enhancement of ethanol yield to 99%.

Collection of concentrated ethanol and system stability

With anodic ethanol loss mechanisms blocked, ethanol can be recovered from the cathode and the porous layer. We carried out experiments to determine the concentration of the ethanol in the cathodic and the porous layer outlet streams using a DI water flow rate of 0.5 mL/min through the porous layer, at room temperature. The concentrations of the ethanol recovered on the cathode and the porous layer were 4.87 wt% and 0.08 wt%, respectively (Figure 3B and Figure S7). The lower concentration from the porous layer can be attributed to three factors. First, the hydroxide/carbonate/bicarbonate ions produced from the CO₂RR on the cathode side combine with the protons produced from oxygen evolution reaction (OER) on the anode side to form water in the porous layer (Figure S8). Second, the anolyte migrates through the CEM—via electroosmosis and diffusion—and this influx dilutes the ethanol inside the porous layer. Third, water added to remove the trapped ethanol further dilutes the stream.

We posited that by tuning the ethanol transport dynamics, a higher concentration of ethanol could be retained at the cathode side. We carried out experiments to control the water transport in the porous layer, and hence alter the concentration of ethanol in the porous layer and reduce the transport of ethanol through the AEM via diffusion. The ethanol concentration in the porous layer can be controlled by supplying either DI water or inert N₂ gas through the layer. Decreasing the flow rate of DI water or tuning the flow rate of N₂ in the porous layer allowed the production of a higher concentration of ethanol in the porous layer. This resulted a lower concentration difference between the cathode and the porous layer and hence slowing down the ethanol diffusion through the AEM. The total ethanol FE produced is unaffected by the fluid or flowrates employed in the porous layer (Figure 3A). However, the cathodic ethanol share (fraction of produced ethanol captured from the cathode stream) increased from 27% at a DI water flow rate of 0.5 mL/min to over 55% when the flow was switched to 25 sccm N₂ (Figure 3A). These conditions led to a higher ethanol concentration, reaching a maximum of 8.6 wt% at a N₂ flow rate of 25 sccm (Figure 3B), a 3.4X improvement compared to the AEM-based MEA. Further increasing the flow rate to 50 sccm N₂ did not yield a higher cathodic ethanol FE nor a higher outlet concentration. The ethanol concentration in the porous layer also increased when a N₂ flow was used, reaching a maximum of 0.5 wt% at a flow rate of 25 sccm N₂ (Figure S7).

We investigated the effect of temperature on the performance of the electrolyzer (Figure S9 and Figure S10). We expected a higher operating temperature to accelerate the evaporation of the produced ethanol on the cathode side. The cathodic share of produced ethanol at 40°C and 60°C were 60% and 66%, respectively (Figure 3C). A maximum cathodic ethanol concentration of 10.5 wt% was achieved at 40°C (Figure 3D) – a concentration exceeding the threshold set by the incumbent industrial ethanol production process, fermentation.^{14,29} Although further increasing the temperature to 60°C further increased the share of ethanol in the cathode, the concentration dropped to 3.6 wt% (Figure 3D). We attributed this lower concentration to a lower cathodic ethanol FE (7.8%) at this temperature and more evaporation of water into the cathodic gas stream at these conditions.

Stability and system optimization

We investigated the stability of the electrolyzer with the porous proton exchange layer. We first performed the experiment at 200 mA/cm² using a DI water flow rate of 0.05 mL/min through the porous layer and pure water as the anolyte. Although the FE for CO₂RR remained relatively constant, the magnitude of the full-cell voltage increased gradually over 4 hours of continuous operation (Figure S13). We attributed this voltage increase to the diffusion of formate, acetate and CO₂ into the anode causing acidification of anolyte and an associated increase in Nernstian voltage. We instead employed a strongly acidic solution (0.01 M H₂SO₄) as the anolyte to provide a stable pH and sufficient conductivity for the anodic OER reaction. Transport CO₂ to the anolyte in conventional AEM-based MEA systems is a major challenge.^{37–40} With the locally acidic condition provided by the porous proton exchange layer²⁵, we measured trace CO₂ to the anode for both DI water and sulfuric acid anolyte cases in our system. With the acid anolyte, we achieved current densities and product selectivities similar to those obtained for DI water (Figure S11), indicating similar cathodic conditions for

both anolyte cases. Operating at 200 mA/cm² with a DI water flow rate of 0.05 mL/min through the porous layer and 0.01 M H₂SO₄ as the anolyte, we achieved a stable ethanol concentration of 7.5 wt% (average) for over 80 hours of continuous operation (Figure 4A). FEs toward all other liquid and gas products of CO₂RR also remained constant over 80 hours of operation (Figure S12). The total ethanol FE and the cathodic ethanol concentration remained over 16% and 7 wt%, respectively, after 80 hours of operation (Figure 4A). The total gas and liquid products collected from the cathode gas outlet and the porous layer approached 100% FE throughout, indicating the suppression of liquid product oxidation and effective blocking of ethanol crossover. To achieve higher ethanol concentrations at the cathodic liquid stream, we further tuned temperature and N₂ flow rate. Employing the N₂ flow rate of 25 sccm and an operating temperature of 40°C, we achieved continuous production of concentrated ethanol at 10 wt% over 5-h of CO₂RR at a constant current density of 200 mA/cm² (Figure S14).

The thickness of the porous proton exchange layer introduced ohmic losses to the system. Therefore, we pursued a lower full-cell voltage by reducing the thickness of the porous layer. Operating with the thinner porous layer (thickness reduced from ~2mm to ~0.75mm) at a temperature of 40°C, the full-cell voltage was significantly reduced, reaching 200 mA/cm² at a voltage of -3.85 V (Figure 4B), a ~450 mV deduction in voltage compared to the thicker porous proton exchange layer running at the same conditions. This voltage is comparable to current state-of-the-art ethanol-producing MEAs with a single membrane.^{8,23,41} We sought to further improve the ethanol concentration by incorporating an AEM with a lower water uptake. Membranes with lower water uptakes have been shown to reduce CO₂RR liquid product crossover and lower water content in the product stream.⁴² Substituting the Sustainion X37-50 membrane with a the low-water-uptake PiperION^{43,44} membrane, we achieved a maximum ethanol concentration of 13.1 wt% directly from the cathode while operating with 40°C and a N₂ flow of 25 sccm through the porous layer. This represents the most concentrated ethanol production from CO₂ electrolysis to date. This system configuration provided stable operation for over 20-h at a voltage of -3.85 V under a fixed current density of 200 mA/cm². The FEs of ethanol and concentration collected at the cathode outlet remained stable over the course of the prolonged experiment (Figure 4B).

Conclusion

We report an approach that eliminates the product loss mechanisms that have limited CO₂-to-ethanol electroconversion to date. We develop a proton exchange layer that creates an electroosmotic flow in the direction opposite to ethanol crossover. This strategy fully blocks the electroosmotic transport and diffusive transport routes, and eliminates the crossover of ethanol to the anode. Owing to its highly porous structure, the electrolyzer enables direct collection of ethanol before reaching to the anode and boosts the ethanol concentrations directly at the cathodic liquid stream. By taking this approach, we effectively block the ethanol loss to the anode (< 1%) and achieve continuous electrosynthesis of concentrated ethanol (exceeding 10 wt%) at the cathode. The electrolyzer with the porous proton exchange layer achieves continuous production of concentrated ethanol of 7.5 wt% for over 80 hours of uninterrupted operation at a constant current density of 200 mA/cm². The strategy reported here presents a viable route to extract liquid fuel at useful concentrations from CO₂ electrolysis.

EXPERIMENTAL PROCEDURES

Resource Availability

Lead Contact

Further information and requests for resources should be directed to and will be fulfilled by the Lead Contact, David Sinton (sinton@mie.utoronto.ca).

Materials Availability

This study did not generate new unique reagents.

Data and Code Availability

The data presented in this work are available from the corresponding authors upon reasonable request.

Electrode Preparation

Cathodes were prepared by sputtering 200 nm of Cu (99.99%) onto a porous PTFE membrane. For the stability experiments, an additional support layer was airbrushed onto the cathodes. The airbrush ink consisted of 40 mg carbon nanoparticles, 350 mg binder (XA-9 Alkaline Ionomer 5% in ethanol, Dioxide Materials) mixed in 1.25 mL methanol. The ink was then sonicated for at least 30 minutes to obtain a homogeneous ink, and airbrushed onto the Cu cathodes to achieve a 0.15 mg/cm² loading. The anodes were prepared by depositing IrO₂ on a titanium mesh support (0.002" thickness, Fuel Cell Store) by a dip coating followed by calcination. The titanium mesh was first rinsed with acetone and DI water, and etched with boiling 0.5 M oxalic acid for 30 minutes. The etched titanium mesh was then dip coated in a solution consists of 30 mg IrCl₃·xH₂O (Alfa Aesar) dissolved in 10 mL isopropanol solution with 10% concentrated HCl. The titanium mesh coated with IrCl₃ was then calcinated at 500°C for 10 minutes. The dipping and calcination processes were repeated until a loading of 1 mg/cm² loading was achieved.

Electrolyzer Configuration

The MEA experiments were performed in an electrolyzer cell (316L stainless steel cathode, and grade 2 titanium anode) with an active area of 5 cm² accessed with a serpentine channel. An anion exchange membrane (Sustainion X37-50 Grade RT, Dioxide Materials or PiperION[™]-A40-HCO₃, Versogen) was sandwiched between the cathode and the anode. Unless otherwise specified, 80 sccm of humidified CO₂ was fed into the cathode using an accurate mass flow controller, while the anode was circulated with 0.1 M KHCO₃ electrolyte at a rate of 5 mL/min with a peristaltic pump. The experiments in the electrolyzer with the porous proton exchange layer were performed in the same electrolyzer with an additional 1.5 mm grade 2 titanium flow field, sealed with two 0.25 mm silicone gaskets. Styrene-divinylbenzene sulfonated copolymer (Dowex 50WX2, 200-400 mesh, Sigma) was used as the porous proton exchange electrolyte. An anion exchange membrane (Sustainion X37-50 Grade RT, Dioxide Materials) and cation exchange membrane (Nafion 117, Fuel Cell Store) were used for ion exchange and separation of the porous proton exchange layer from the cathode and anode, respectively. Unless otherwise specified, 80 sccm of humidified CO₂ was fed into the cathode while the anode was circulated with either DI water or 0.01 M H₂SO₄ electrolyte at a rate of 5 mL/min. Either DI water or inert N₂ gas was used as the carrier to release the liquid products collected in the porous proton exchange layer. For the experiment with the thinner porous layer, a 0.75 mm (measured without compression) silicone sheet was laser cut with channels and used as the flow field.

Product Analysis

Gas products were taken from the cathode outlet and analyzed with a gas chromatograph (PerkinElmer Clarus 590) coupled with a thermal conductivity detector and flame ionization detector. The liquid products were collected separately from the cathode and the porous proton exchange layer outlet using cold traps cooled in a water bath at 0°C. The liquid products from the cold traps and the anolyte were quantified using proton nuclear magnetic resonance spectroscopy (¹H⁺ NMR) using water suppression mode, with dimethyl sulfoxide (DMSO) as the internal standard.

The FE of each gas product was calculated using the same method as prior report⁴⁵:

$$FE_{gas} = x_i \times v \times \frac{z_i F P_o}{RT} \times \frac{1}{I_{total}} \times 100\%$$

The FE of each liquid product was calculated as follows:

$$FE_{liquid} = n_i \times v \times \frac{z_i F}{Q} \times 100\%$$

where x_i represents the volume fraction of gas product i , v represents the gas flow rate at the outlet in sccm, z_i represents the number of electrons required to produce one molecule of product i , F represents the Faraday constant, P_o represents atmospheric pressure in Pa, R represents the ideal gas constant, T represents the temperature, and I_{total} represents the total current; n_i represents the number of moles of product i , and Q represents the charged passed while the liquid products are being collected.

SUPPLEMENTAL INFORMATION

ACKNOWLEDGMENTS

The authors acknowledge support and infrastructure from the Natural Sciences and Engineering Research Council (NSERC), the Government of Ontario through the Ontario Research Fund. This work is supported by Suncor Energy Ltd and the NSERC Alliance grant program. R.K.M. thanks NSERC, Hatch, and the Government of Ontario for their support through graduate scholarships. Y.X. thanks NSERC for support in the form of a graduate scholarship. Infrastructure provided by the Canada Foundation for Innovation (CFI) and the Ontario Research Fund (ORF) is gratefully acknowledged.

AUTHOR CONTRIBUTIONS

R.K.M. designed and carried out all experiments, as well as prepared the manuscript with advice from Y.X., Y.X., A.R. and G.L., assisted in experimental setup and data analysis. C.P.O., C.M.G., J.P.E. and S.L. assisted in the MEA experiments. J.E.H., X.W., and Y.Y. prepared the Cu electrodes. Y.X. and M.F. assisted in the experiments with the thinner porous layer. A.O., E.H.S. and D.S. contributed to manuscript editing. E.H.S. and D.S. supervised the project. All authors discussed the results and assisted during the manuscript preparation.

DECLARATION OF INTERESTS

The authors declare no competing interests.

Main Figures

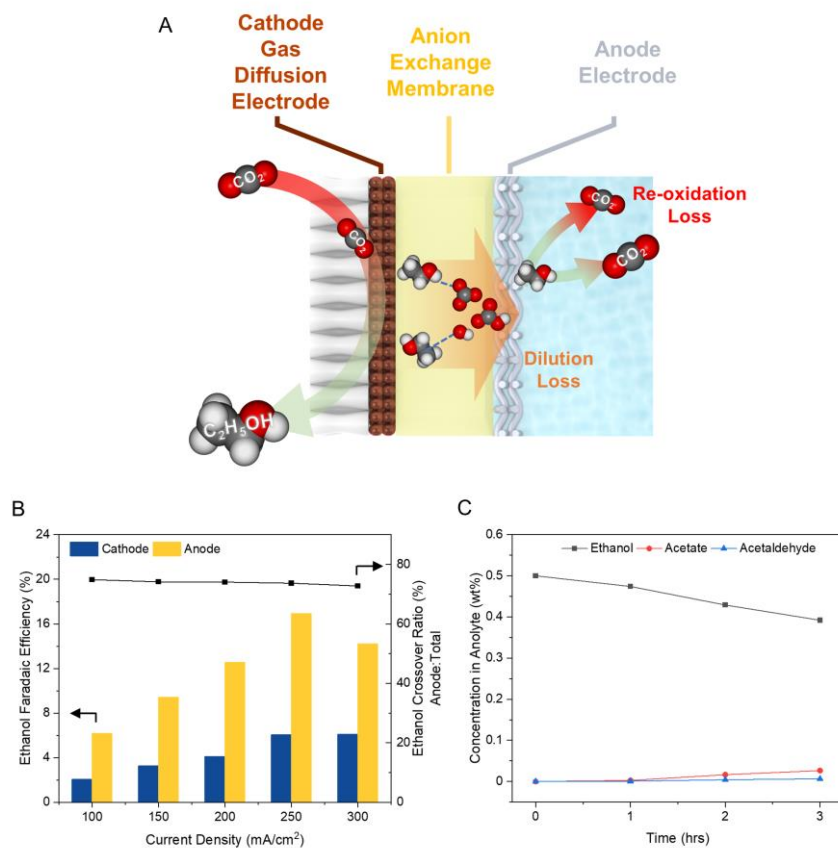


Figure 1. Crossover in the MEA (A) Schematic illustration of ethanol loss mechanisms in the conventional MEA electrolyzer, (B) Cathode vs. anode ethanol distribution for an MEA, (C) Ethanol oxidation experiment with 0.5 wt% initial ethanol concentration added to the anolyte.

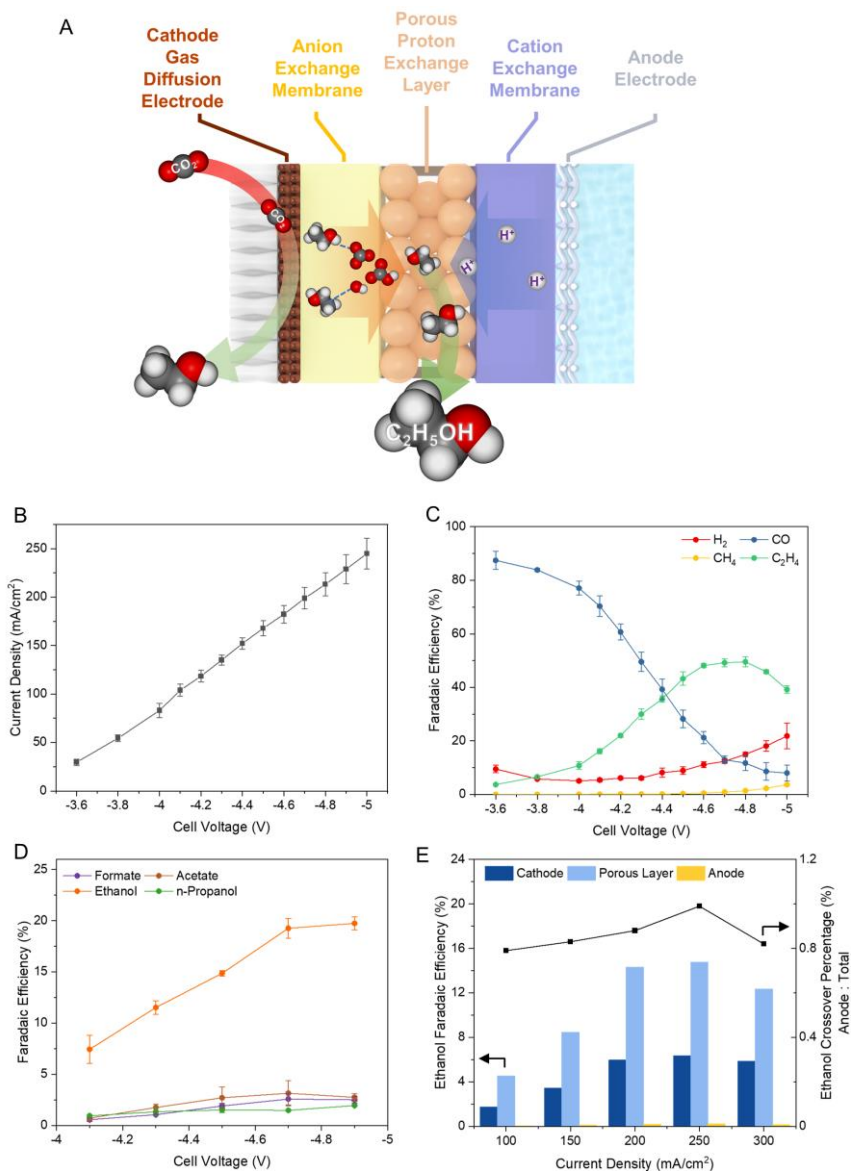


Figure 2. Performance of the electrolyzer with the porous proton exchange layer (A) Schematic illustration the electrolyzer with the porous layer, (B) Relationship between current density and applied full-cell voltage for the electrolyzer with the porous layer, (C) Gas product selectivity for the electrolyzer with the porous layer, (D) Liquid product selectivity for the electrolyzer with the porous layer, (E) Ethanol distribution for the electrolyzer with the porous layer. The error bars correspond to the standard deviation of at least three independent measurements.

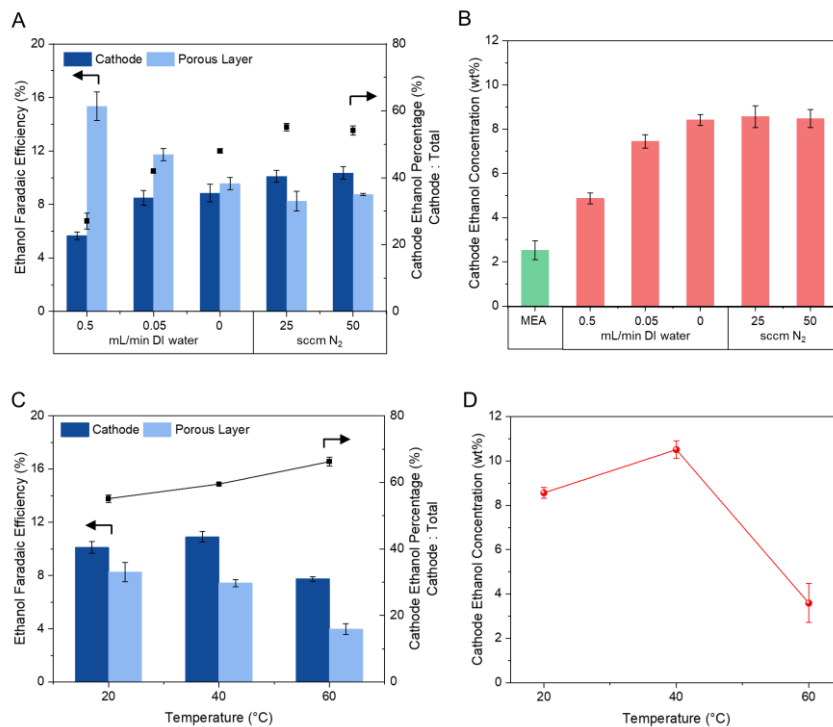


Figure 3. Effect of flow rate through the porous layer and temperature on cathodic ethanol concentration (A) Ethanol FE and distribution for different DI water and N₂ flow rates in the porous layer, (B) Cathodic ethanol concentration at different DI water or N₂ flow rates, (C) Relationship between cell operation temperature and the ethanol FE distribution, (D) Cathodic ethanol concentration at different cell operation temperatures. The error bars correspond to the standard deviation of at least three independent measurements.

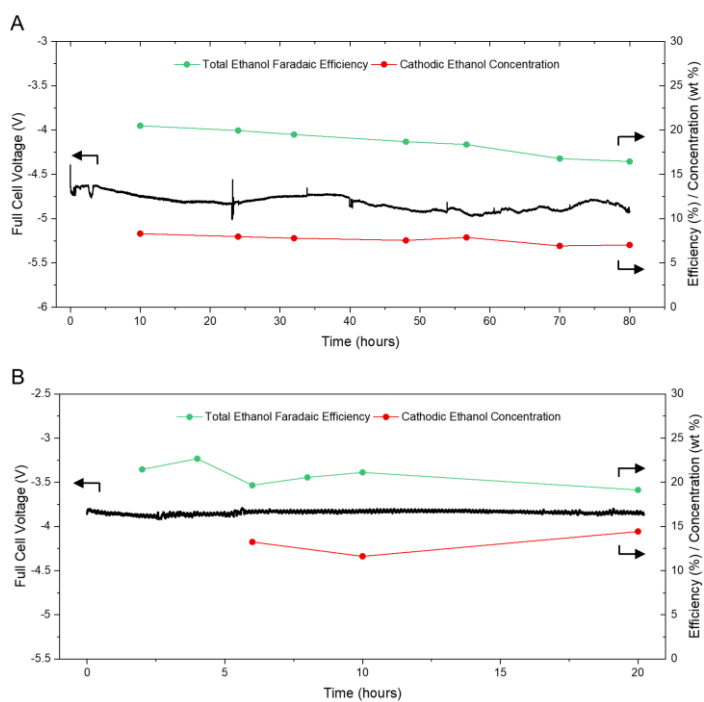


Figure 4. System Stability (A) Voltage and product stability for a prolonged experiment run at 200 mA/cm² with 0.05 mL/min DI water flow rate through the porous layer and 0.01 M H₂SO₄ as the anolyte, (B) Voltage and product stability for the system with the thinner porous proton exchange layer at 200 mA/cm² with 25 sccm N₂ through the porous layer and 0.01 M H₂SO₄ as the anolyte at an operating temperature 40°C (The periodic cycle shown on the graph is caused by on/off heating cycle controlled by a PID controller).

REFERENCES

- Bushuyev, O.S., De Luna, P., Dinh, C.T., Tao, L., Saur, G., van de Lagemaat, J., Kelley, S.O., and Sargent, E.H. (2018). What Should We Make with CO₂ and How Can We Make It? *Joule* 2, 825–832.
- Jhong, H.R.M., Ma, S., and Kenis, P.J. (2013). Electrochemical conversion of CO₂ to useful chemicals: Current status, remaining challenges, and future opportunities. *Curr. Opin. Chem. Eng.* 2, 191–199.
- De Luna, P., Hahn, C., Higgins, D., Jaffer, S.A., Jaramillo, T.F., and Sargent, E.H. (2019). What would it take for renewably powered electrosynthesis to displace petrochemical processes? *Science* 364, eaav3506.
- Whipple, D.T., and Kenis, P.J.A. (2010). Prospects of CO₂ utilization via direct heterogeneous electrochemical reduction. *J. Phys. Chem. Lett.* 1, 3451–3458.
- Spurgeon, J.M., and Kumar, B. (2018). A comparative technoeconomic analysis of pathways for commercial electrochemical CO₂ reduction to liquid products. *Energy Environ. Sci.* 11, 1536–1551.
- Kibria, M.G., Edwards, J.P., Gabardo, C.M., Dinh, C.-T., Seifitokaldani, A., Sinton, D., and Sargent, E.H. (2019). Electrochemical CO₂ Reduction into Chemical Feedstocks: From Mechanistic Electrocatalysis Models to System Design. *Adv. Mater.* 31, 1807166.
- H. Shapouri, J. A. Duffield, and M. Wang (2003). THE ENERGY BALANCE OF CORN ETHANOL REVISITED. *Trans. ASAE* 46, 959–968.
- Wang, X., Wang, Z., Arquer, F.P.G. de, Dinh, C.-T., Ozden, A., Li, Y.C., Nam, D.-H., Li, J., Liu, Y.-S., Wicks, J., et al. (2020). Efficient electrically powered CO₂ to ethanol via suppression of deoxygenation. *Nat. Energy* 5, 478–486.
- Li, Y.C., Wang, Z., Yuan, T., Nam, D.H., Luo, M., Wicks, J., Chen, B., Li, J., Li, F., De Arquer, F.P.G., et al. (2019). Binding Site Diversity Promotes CO₂ Electroreduction to Ethanol. *J. Am. Chem. Soc.* 141, 8584–8591.
- Li, F., Li, Y.C., Wang, Z., Li, J., Nam, D.H., Lum, Y., Luo, M., Wang, X., Ozden, A., Hung, S.F., et al. (2020). Cooperative CO₂-to-ethanol conversion via enriched intermediates at molecule–metal catalyst interfaces. *Nat. Catal.* 3, 75–82.
- Weng, L.C., Bell, A.T., and Weber, A.Z. (2019). Towards membrane-electrode assembly systems for CO₂ reduction: A modeling study. *Energy Environ. Sci.* 12, 1950–1968.
- Salvatore, D., and Berlinguette, C.P. (2020). Voltage Matters When Reducing CO₂ in an Electrochemical Flow Cell. *ACS Energy Lett.* 5, 215–220.
- Gabardo, C.M., O'Brien, C.P., Edwards, J.P., McCallum, C., Xu, Y., Dinh, C.T., Li, J., Sargent, E.H., and Sinton, D. (2019). Continuous Carbon Dioxide Electroreduction to Concentrated Multi-carbon Products Using a Membrane Electrode Assembly. *Joule* 3, 2777–2791.
- Greenblatt, J.B., Miller, D.J., Ager, J.W., Houle, F.A., and Sharp, I.D. (2018). The Technical and Energetic Challenges of Separating (Photo)Electrochemical Carbon Dioxide Reduction Products. *Joule* 2, 381–420.
- Jouny, M., Luc, W., and Jiao, F. (2018). General Techno-Economic Analysis of CO₂ Electrolysis Systems. *Ind. Eng. Chem. Res.* 57, 2165–2177.
- Li, Y.C., Yan, Z., Hitt, J., Wycisk, R., Pintauro, P.N., and Mallouk, T.E. (2018). Bipolar Membranes Inhibit Product Crossover in CO₂ Electrolysis Cells. *Adv. Sustain. Syst.* 2, 1700187.
- Zhang, J., Luo, W., and Züttel, A. (2020). Crossover of liquid products from electrochemical CO₂ reduction through gas diffusion electrode and anion exchange membrane. *J. Catal.* 385, 140–145.
- Wang, N., Miao, R.K., Lee, G., Vomiero, A., Sinton, D., Ip, A.H., Liang, H., and Sargent, E.H. (2021). Suppressing the liquid product crossover in electrochemical CO₂ reduction. *SmartMat*, smm2.1018.
- Kibria Nabil, S., McCoy, S., and Kibria, M.G. (2021). Comparative life cycle assessment of electrochemical upgrading of CO₂ to fuels and feedstocks. *Green Chem.* 23, 867–880.
- Baeyens, J., Kang, Q., Appels, L., Dewil, R., Lv, Y., and Tan, T. (2015). Challenges and opportunities in improving the production of bio-ethanol. *Prog. Energy Combust. Sci.* 47, 60–88.
- Ripatti, D.S., Veltman, T.R., and Kanan, M.W. (2019). Carbon Monoxide Gas Diffusion Electrolysis that Produces Concentrated C₂ Products with High Single-Pass Conversion. *Joule* 3, 240–256.
- Lee, W., Kim, Y.E., Youn, M.H., Jeong, S.K., and Park, K.T. (2018). Catholyte-Free Electrocatalytic CO₂ Reduction to Formate. *Angew. Chemie - Int. Ed.* 57, 6883–6887.
- Grigioni, I., Sagar, L.K., Li, Y.C., Lee, G., Yan, Y., Bertens, K., Miao, R.K., Wang, X., Abed, J., Won, D.H., et al. (2020). CO₂ Electroreduction to Formate at a Partial Current Density of 930 mA cm⁻² with InP Colloidal Quantum Dot Derived Catalysts. *ACS Energy Lett.* 28, 79–84.

24. Fan, L., Xia, C., Zhu, P., Lu, Y., and Wang, H. (2020). Electrochemical CO₂ reduction to high-concentration pure formic acid solutions in an all-solid-state reactor. *Nat. Commun.* *11*, 1–9.
25. Yang, H., Kaczur, J.J., Sajjad, S.D., and Masel, R.I. (2017). Electrochemical conversion of CO₂ to formic acid utilizing Sustainion™ membranes. *J. CO₂ Util.* *20*, 208–217.
26. Xia, C., Zhu, P., Jiang, Q., Pan, Y., Liang, W., Stavitskiy, E., Alshareef, H.N., and Wang, H. (2019). Continuous production of pure liquid fuel solutions via electrocatalytic CO₂ reduction using solid-electrolyte devices. *Nat. Energy* *4*, 776–785.
27. Courtois, J., Du, W., Wong, E., Teng, X., and Deskins, N.A. (2014). Screening iridium-based bimetallic alloys as catalysts for direct ethanol fuel cells. *Appl. Catal. A Gen.* *483*, 85–96.
28. Du, W., Deskins, N.A., Su, D., and Teng, X. (2012). Iridium-ruthenium alloyed nanoparticles for the ethanol oxidation fuel cell reactions. *ACS Catal.* *2*, 1226–1231.
29. Camara, G.A., and Iwasita, T. (2005). Parallel pathways of ethanol oxidation: The effect of ethanol concentration. *J. Electroanal. Chem.* *578*, 315–321.
30. Wang, H., Jusys, Z., and Behm, R.J. (2004). Ethanol electrooxidation on a carbon-supported Pt catalyst: Reaction kinetics and product yields. *J. Phys. Chem. B* *108*, 19413–19424.
31. Li, X., Zhang, H., Mai, Z., Zhang, H., and Vankelecom, I. (2011). Ion exchange membranes for vanadium redox flow battery (VRB) applications. *Energy Environ. Sci.* *4*, 1147–1160.
32. Goyal, A., Marcandalli, G., Mints, V.A., and Koper, M.T.M. (2020). Competition between CO₂ Reduction and Hydrogen Evolution on a Gold Electrode under Well-Defined Mass Transport Conditions. *J. Am. Chem. Soc.* *142*, 4154–4161.
33. Dinh, C.T., Burdyny, T., Kibria, G., Seifitokaldani, A., Gabardo, C.M., Pelayo García De Arquer, F., Kiani, A., Edwards, J.P., De Luna, P., Bushuyev, O.S., et al. (2018). CO₂ electroreduction to ethylene via hydroxide-mediated copper catalysis at an abrupt interface. *Science* (80-.). *360*, 783–787.
34. Tan, Y.C., Lee, K.B., Song, H., and Oh, J. (2020). Modulating Local CO₂ Concentration as a General Strategy for Enhancing C–C Coupling in CO₂ Electroreduction. *Joule* *4*, 1104–1120.
35. Xu, Y., Edwards, J.P., Liu, S., Miao, R.K., Huang, J.E., Gabardo, C.M., O'Brien, C.P., Li, J., Sargent, E.H., and Sinton, D. (2021). Self-Cleaning CO₂ Reduction Systems: Unsteady Electrochemical Forcing Enables Stability. *ACS Energy Lett.* *6*, 809–815.
36. Fan, L., Xia, C., Yang, F., Wang, J., Wang, H., and Lu, Y. (2020). Strategies in catalysts and electrolyzer design for electrochemical CO₂ reduction toward C₂+ products. *Sci. Adv.* *6*, eaay3111.
37. Ozden, A., Wang, Y., Li, F., Luo, M., Sisler, J., Thevenon, A., Rosas-Hernández, A., Burdyny, T., Lum, Y., Yadegari, H., et al. (2021). Cascade CO₂ electroreduction enables efficient carbonate-free production of ethylene. *Joule* *5*, 706–719.
38. Huang, J.E., Li, F., Ozden, A., Rasouli, A.S., Arquer, F.P.G. de, Liu, S., Zhang, S., Luo, M., Wang, X., Lum, Y., et al. (2021). CO₂ electrolysis to multicarbon products in strong acid. *Science* (80-.). *372*, 1074–1078.
39. Chen, C., Li, Y., and Yang, P. (2021). Address the “alkalinity problem” in CO₂ electrolysis with catalyst design and translation. *Joule* *5*, 737–742.
40. Dinh, C.T., Li, Y.C., and Sargent, E.H. (2019). Boosting the Single-Pass Conversion for Renewable Chemical Electrosynthesis. *Joule* *3*, 13–15.
41. Gu, Z., Shen, H., Chen, Z., Yang, Y., Yang, C., Ji, Y., Wang, Y., Zhu, C., Liu, J., Li, J., et al. (2021). Efficient Electrocatalytic CO₂ Reduction to C₂+ Alcohols at Defect-Site-Rich Cu Surface. *Joule* *5*, 429–440.
42. Salvatore, D.A., Gabardo, C.M., Reyes, A., O'Brien, C.P., Holdcroft, S., Pintauro, P., Bahar, B., Hickner, M., Bae, C., Sinton, D., et al. (2021). Designing anion exchange membranes for CO₂ electrolyzers. *Nat. Energy* *6*, 339–348.
43. Wang, J., Zhao, Y., Setzler, B.P., Rojas-Carbonell, S., Ben Yehuda, C., Amel, A., Page, M., Wang, L., Hu, K., Shi, L., et al. (2019). Poly(aryl piperidinium) membranes and ionomers for hydroxide exchange membrane fuel cells. *Nat. Energy* *4*, 392–398.
44. Zhao, Y., Setzler, B.P., Wang, J., Nash, J., Wang, T., Xu, B., and Yan, Y. (2019). An Efficient Direct Ammonia Fuel Cell for Affordable Carbon-Neutral Transportation. *Joule* *3*, 2472–2484.
45. Ma, M., Clark, E.L., Therkildsen, K.T., Dalsgaard, S., Chorkendorff, I., and Seger, B. (2020). Insights into the carbon balance for CO₂ electroreduction on Cu using gas diffusion electrode reactor designs. *Energy Environ. Sci.* *13*, 977–985.